



Mediating interaction strength between nickel and zirconia using a mixed oxide nanosheets interlayer for methane dry reforming

Anup P. Tathod^a, Naseem Hayek^a, Dina Shpasser^a, David S.A. Simakov^b, Oz M. Gazit^{a,*}

^a Faculty of Chemical Engineering, Technion, Israel Institute of Technology, Haifa 3200003, Israel

^b Department of Chemical Engineering, University of Waterloo, Waterloo, ON, N2L 3G1, Canada



ARTICLE INFO

Keywords:

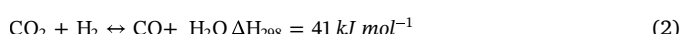
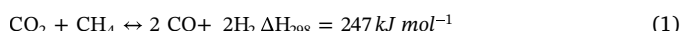
Methane dry reforming
Hydrotalcite
Layered double hydroxide nanosheet
Nickel catalyst
Metal-support interaction
Surface phase oxide
Surface thin oxides

ABSTRACT

For many reactions balancing the degree of interaction between the metal catalyst and the underlying support material is pivotal for obtaining optimal catalytic performance. One important example is the reforming of methane contained in biogas, using CO₂ as an oxidizer, to make syngas (H₂ and CO). For this reaction to become industrially viable, the catalyst needs to be based on non-precious transition metals. Unfortunately, catalyst deactivation induced by metal sintering and coking remains a major challenge for this class of catalysts. Herein, we demonstrate the use of a "surface phase oxide" in the form of MgAl mixed oxide nanosheets (< 2 nm thick), derived from layered double hydroxide, as an interlayer to mediate the interaction between nickel nanoparticles and an underlying zirconia support. This unique hierarchical catalyst configuration is shown to enhance conversion, under undiluted conditions and GHSV = 240,000 cm³h⁻¹g_{cat}⁻¹, by up to 2-fold, as compared to Ni supported on ZrO₂ and by up to 15-fold as compared to Ni on bulk MgAl mixed oxide, keeping the catalyst stable over 240 h reaction times. To gain better understanding into the mechanism of enhanced catalytic performance we used a combination of PXRD, SAXS, Cryo-TEM, H₂-TPR, STEM-EDS, and XPS in conjunction with the results for the catalytic performance. The combined results show that the amplified catalytic performance is strongly correlated with the modification of the metal-support interaction (MSI) by the MgAl mixed oxide interlayer. Although the physical interaction of Ni particles at the edges of the nanosheets with the underlying ZrO₂ cannot be completely dismissed, all the available data shows no such interaction exists. Hence, the change in MSI in the stacked configuration is attributed to the indirect MSI effect of the underlying ZrO₂ on the properties of the nickel catalyst. Overall the approach described here, for manipulating MSI to promote the challenging methane dry reforming, can be extended by replacing the underlying metal oxide support (commercial or custom made), synthesis of mixed oxide nanosheets of different A²⁺B³⁺ ratios and type, and changing the active metal catalyst.

1. Introduction

Conversion of methane and carbon dioxide contained in natural gas or biogas [1,2] into value added chemicals has recently attracted much attention [2]. Among the most promising routes is methane reforming using CO₂ as an oxidant, i.e., methane dry reforming (MDR), to make syngas (H₂ + CO), see Eq. (1). The MDR reaction is reversible and always accompanied by the mildly endothermic reverse water gas shift (RWGS) reaction, Eq. (2).



The syngas can then be converted in subsequent processes into a variety of fuels and chemicals, including methanol and synthetic oil (via

the Fischer-Tropsch process) [3]. However, the MDR process is currently not performed on a commercial scale, predominantly due to the limitations imposed by process performance and economics of currently available catalysts [2,4,5].

The harsh MDR conditions (~1000–1200 °C to achieve ~80–100% conversion) require the use of noble metals as catalysts, which is a major hurdle for commercialization due to the limited availability and high cost of platinum group metals [6–9]. The advantage of using noble metals such as Pt, Rh and Ru is their high activity and resistance to coke deposition and sintering [10–14]. As a low cost alternative, Ni-based formulations were identified as active catalysts for MDR [7,15–20]. However, unlike noble metals, for which the Tamman temperature (T_{Tam}) is above the thermodynamically desired reaction temperature (at least 600–800 °C), Ni has a lower T_{Tam} (590 °C). As a result, Ni

* Corresponding author at: Faculty of Chemical engineering, Technion, Israel Institute of Technology, Haifa, 3200003, Israel.
E-mail address: ozg@technion.ac.il (O.M. Gazit).

nanoparticles are highly prone to sintering under the MDR reaction conditions. Moreover, the presence of high concentrations of carbon species in MDR makes the deactivation of Ni by carbon deposition a thermodynamically favorable path [8]. The latter stimulates the use of even higher reaction temperatures to limit carbon formation [21] but also promotes the sintering of Ni nanoparticles.

Studies have shown that supported Ni nanoparticles with a small size (< 5 nm) are more resistant to coke formation in MDR [22–24]. However, because of the low T_{Tam} , maintaining the high degree of Ni dispersion is a non-trivial task. One possible option is to select a support (e.g., metal oxide) that has strong interaction with an active metallic phase. In this case, the metal oxide support can play a key role as a stabilizer and/or promoter, acting as a surrogate ligand for coordinately unsaturated surface sites [25–28]. These effects will become more pronounced with the decrease in size of the supported metal catalyst, which enhances the interaction with the underlying support and, in turn, the effect of the support on reaction activity and selectivity [29]. Under MDR conditions, with temperatures exceeding 600 °C and reducing atmosphere, such strong interaction with the underlying support may block active sites, e.g. by overgrowth of a reducible support material on top of the catalytic metal particle [30]. An example for this effect was shown by Tauster et al. for the overgrowth of TiO₂ on Pd catalyst, which reduced the measured catalyst dispersion while no metal particle sintering occurred. This effect is typically termed strong metal support interaction (SMSI) [31,32]. Several recent papers have highlighted the importance of controlling the strength of these interactions as a tool for obtaining enhanced catalytic stability while keeping high activity [33–38].

The use of a support with an intrinsic basicity such as hydrotalcites (mixed oxide) was shown to suppress carbon deposition in MDR by promoting stronger chemisorption of the acidic CO₂ [39,40]. MDR catalysts prepared using hydrotalcite like materials, LDH derived mixed oxides and spinels, as either catalyst precursors or a support materials, have shown high dispersion of active sites, good resistance to coke formation and good thermal stability [19,39,41–44]. These beneficial properties result from a strong interaction between the metallic phase and the basic support, which in turn requires very high temperatures for full reduction of the Ni phase (~800–850 °C) [19]. The reduction temperature of Ni supported on a metal oxide such as zirconia, which interacts more weakly with NiO, is much lower ~450 °C (close to the reduction temperature of bulk nickel oxide ~350 °C) [45].

Different approaches for stabilizing Ni on metal oxides/supports exist. These include confining, embedding or encapsulating within well-defined small pores/cavities or by creation of a confining environment, which leverages on metal-support interactions (MSI) [28,46,47]. All these methods were thoroughly reviewed recently by Shuirong Li and Jinlong Gong [48]. The downsides of these approaches are the introduction of mass transport limitation, more limited site accessibility and high temperatures of NiO reduction, which promotes sintering.

Roughly three decades ago, an approach based on a 'surface phase oxide', was studied by Wachs and co-workers [49] and Ko and co-workers [50,51]. Ko et al. investigated the interaction of Ni with a monolayer of TiO₂ deposited on a SiO₂ surface. The authors showed that the deposition of a strongly interacting support (TiO₂) on a weakly interacting oxide (SiO₂) inflicted change in MSI such that Ni on TiO₂/SiO₂ exhibited weaker MSI than Ni on bulk TiO₂ [50]. The same authors demonstrated a similar effect with Ni supported on Nb₂O₅/SiO₂ [51]. Despite the promising results obtained using this approach, no progress has been made since.

Here, we extend the approach instigated by Ko and co-workers to amplify the catalytic performance of Ni by dispersing the Ni phase on nanosheets of MgAl mixed oxide (NS), which are supported on ZrO₂ as an underlying support. The hierarchical system is designated here as Ni/NS/Zr. The Ni on ZrO₂ system (Ni/Zr) was chosen as an example for weak MSI with Ni, as opposed to the strong MSI of Ni with LDH-derived mixed oxide. Herein, we show that a unique stacked hierarchical

configuration can significantly enhance the activity of the Ni phase in MDR, by maintaining high dispersion together with medium strength MSI. Moreover, we show that, despite the fact that Ni was dispersed on the nanosheets of mixed oxide, the selectivity in MDR reaction followed that characteristic to Ni/Zr. Specific attention is given to understanding the interaction between the metallic Ni phase and the oxide support and its effects on the MDR catalytic performance.

2. Experimental section

2.1. Materials

All chemicals were used as received without any further purification. Magnesium nitrate hexahydrate ($\geq 99\%$ purity), aluminum nitrate nonahydrate ($\geq 98\%$) and zirconium oxide (99%) were purchased from Sigma-Aldrich (USA). Nickel nitrate hexahydrate ($\geq 98\%$) was purchased from Strem Chemicals (USA). Sodium nitrate, sodium hydroxide solution and formamide were purchased from Merk KGaA (Germany).

2.2. Preparation of Ni/Zr and Ni/MO

The ZrO₂ support was dried at 150 °C for 3 h prior to use. The MgAl layered double hydroxide (Mg:Al = 4) was prepared according to the quick addition method reported before followed by calcination [52]. Briefly, magnesium nitrate hexahydrate and aluminum nitrate nonahydrate were dissolved in 10 ml of deionized water to obtain a Mg:Al ratio of 4 and a total metal concentration of 0.25 M. The metal precursor solution was then injected into a 500 ml NaOH solution (initial pH 12) containing 0.42 g of NaNO₃ under vigorous stirring (1400 rpm). Upon complete addition of the metal precursor solution, the obtained slurry was stirred for 1 min followed by centrifugation to obtain a gel like mass of layered double hydroxide (LDH). The gel like mass was washed with deionized water three times and dried at 80 °C for 12 h. The dried powder was calcined at 600 °C under air (20 ml/min) for 8 h. The MgAl mixed oxide (MO) obtained after calcination of MgAl LDH was used as a support to prepare Ni/MO catalysts.

Ni/Zr and Ni/MO were prepared by wet impregnation wherein aqueous solution of Ni(NO₃)₂·6H₂O was added to a suspension of support (1 g support in 10 ml water) and stirred for 16 h. The amount of the Ni precursor added was calculated to obtain a desired Ni loading. After stirring the solvent was evaporated using rotary vacuum evaporator. The samples were dried at 80 °C overnight and calcined at 600 °C for 8 h under air flow.

2.3. Preparation of Ni/NS/Zr

The synthesis procedure for the LDH-NSs was identical to that described in Section 2.2, except for the addition of formamide to the base (NaOH) solution during the synthesis, following a modified synthesis protocol reported by Yu and coworkers [53]. The 500 ml base solution was prepared by adding NaOH to a 23% aq. solution of formamide (vol/vol) containing 0.42 g NaNO₃ until pH = 12 was achieved. The following steps in the procedure were identical to those described in Section 2.2 to obtain a gel like mass of the LDH-NSs. After centrifugation and washing, this gel like precipitate was dispersed in 200 ml water to prepare a suspension.

In the second step, 10 g of dried ZrO₂ were added to the above-mentioned suspension of the LDH-NSs to anchor the LDH-NSs onto the surface to prepare LDH-NS/Zr. After stirring the mixture for 16 h at room temperature, the solvent was evaporated using rotary vacuum evaporator. The obtained precipitate was dried overnight at 80 °C and calcined at 600 °C for 8 h under air flow. Upon calcination the LDH transforms into the mixed oxide of MgAl and is grafted onto the ZrO₂ surface. This thin nanosheet of MgAl mixed oxide grafted on the ZrO₂ surface is represented as NS/Zr throughout the manuscript. The NS/Zr was impregnated with Ni in the range of 0.5–10 wt% by wet

Table 1

List of synthesized catalysts with corresponding Ni contents.

Sr. No.	Sample Id	Ni content Nominal (wt%)	Ni content Actual (wt%) ^a
1	10Ni/Zr	10.0	9.49
2	2.5Ni/Zr	2.5	2.29
3	10Ni/MO	10.0	9.61
4	2.5Ni/MO	2.5	2.13
5	10Ni/NS/Zr	10.0	8.23
6	5Ni/NS/Zr	5.0	4.43
7	2.5Ni/NS/Zr	2.5	1.89
8	1Ni/NS/Zr	1.0	0.91
9	0.5Ni/NS/Zr	0.5	0.43

^a Determined using ICP-OES.

impregnation. An aq. solution of $\text{Ni}(\text{NO}_3)_2 \cdot 6\text{H}_2\text{O}$ was added to an aqueous suspension of the support and stirred for 16 h. After stirring the mixture was centrifuged and the solid residue was washed with water twice. All impregnated samples were calcined at 600 °C for 8 h under air flow. All synthesized catalysts are listed in Table 1.

2.4. Characterization techniques and methods

Surface area of the support materials was determined by N_2 -physisorption using a 3-Flex, Micromeritics instrument. All samples were degassed at 150 °C for 6 h under vacuum prior to N_2 adsorption. Metal content was measured by ICP-OES using a Thermo Scientific ICAP 6300 Duo spectrometer. Prior to analysis, accurately weighed samples were dissolved in freshly prepared aqua regia and diluted with deionized water. An aqueous suspension of the LDH-NSs was analyzed by small angle X-ray scattering (SAXS) to determine the thickness of the nanosheets using a Molecular Metrology SAXS system with Cu K α radiation from a sealed micro-focus tube (MicroMax-002 + S, 45 kV, 0.8 mA), two Gobel mirrors and three-pinhole slits.

Temperature programmed reduction experiments (TPR) were performed on a Micromeritics Autochem II instrument. In a typical experiment, the sample was heated in-situ up to 900 °C with a heating rate of 5 °C/min in the flow of air (30 ml/min). Then the sample was cooled down to 50 °C in a flow of Ar. The sample was then heated up to 900 °C in a flow of 10 v:v% H_2 in Ar (20 ml/min) with a heating rate of 15 °C min⁻¹. HAADF-STEM-EDS analysis was performed using an FEI Titan 80–300KeV instrument. The STEM samples were prepared by placing a drop of the aqueous suspension of the sample on the copper grid. Cryo-TEM images of aqueous suspension of the LDH-NSs were recorded on an FEI Tecnai T12 G² instrument. XRD patterns of dried powders were recorded on a Rigaku miniflex II X-ray diffractometer equipped with a Cu-K α (1.54 Å) X-ray source with a scanning rate of 3° min⁻¹. X-ray Photoelectron Spectroscopy (XPS) was performed in UHV (2.5×10^{-10} Torr base pressure) using a 5600 Multi-Technique System (PHI, USA). The samples were irradiated with an Al K α monochromated source (1486.6 eV) and the outcome electrons were analyzed by a Spherical Capacitor Analyzer using a slit aperture of 0.8 mm. C1s at 285.0 was taken as an energy reference for all peaks.

2.5. Catalytic performance evaluation

Catalytic activity was evaluated at 800 °C and atmospheric pressure in a fixed-bed quartz tubular reactor (internal diameter 7 mm). In a typical run, 25 mg of a catalyst (60–100 mesh particle size) diluted with 175 mg of quartz particles (60–70 mesh particle size) was placed on a plug of quartz wool to form a 2.5 mm high catalyst bed inside the reactor. A quartz-sealed K-type thermocouple was fixed inside the reactor above the catalyst bed to ensure the same inlet temperature for all catalysts. Each catalyst was reduced in-situ prior to catalytic testing at a pre-determined temperature of 600 °C or 800 °C for 1 h under a flow of 10 v:v % H_2 in Ar (40 ml min⁻¹ flow rate). The reactor was heated to

800 °C under a flow of Ar. A mixture of CO_2 and CH_4 was passed through the reactor at a total flow of 100 ml min⁻¹ (1:1 $\text{CO}_2:\text{CH}_4$, controlled by Brooks SLA5850 MFCs), which corresponded to $\text{GHSV} = 240,000 \text{ cm}^3 \text{ h}^{-1} \text{ g}_{\text{cat}}^{-1}$. The products were analyzed using an online GC [Clarus 580 (PerkinElmer)] equipped with a TCD detector. The change in total flow rate during reaction was calculated based on total carbon balanced and validated by running the same reactions using 4% v:v N_2 as an internal standard. Based on these experiments the total mass balance of the reaction was validated to close by above 95%. CH_4 and CO_2 conversion (X_{CH_4} , X_{CO_2}) and the outlet H_2/CO ratio were calculated as follows (subscripts *in* and *out* refer to inlet and outlet molar flow rates, respectively):

$$X_{\text{CH}_4} = \frac{F_{\text{CH}_4\text{in}} - F_{\text{CH}_4\text{out}}}{F_{\text{CH}_4\text{in}}} \quad (3)$$

$$X_{\text{CO}_2} = \frac{F_{\text{CO}_2\text{in}} - F_{\text{CO}_2\text{out}}}{F_{\text{CO}_2\text{in}}} \quad (4)$$

$$\frac{\text{H}_2}{\text{CO}} = \frac{F_{\text{H}_2\text{out}}}{F_{\text{CO}\text{out}}} \quad (5)$$

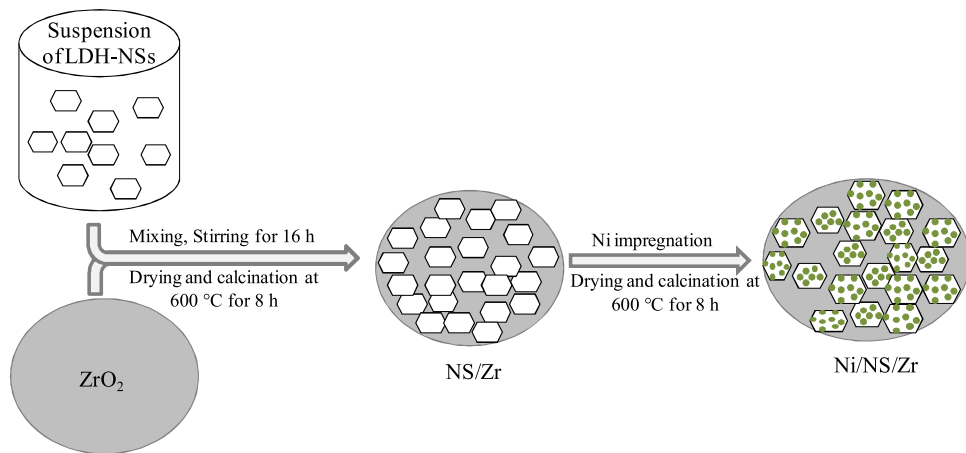
3. Results and discussion

3.1. Catalytic evaluation

We recently reported a protocol for the synthesis of LDH nanoparticles [52]. Modifying this protocol by adding formamide allowed us to quickly and reproducibly make LDH nanosheets (LDH-NS). Cryo-transmission electron microscopy (cryo-TEM) images of the as prepared LDH-NSs showed that the NSs had a lateral diameter in the range of 10–30 nm and a thickness of ~2 nm, see Figure S1. These dimensions were corroborated by fitting a mathematical model describing short cylinders [54] to the small angle X-ray scattering (SAXS) data measured for the NSs suspension, see Figure S2. The SAXS analysis gave an approximate 1.9 nm thickness of the LDH NSs with an average diameter of 14.4 nm. These results are in agreement with the results of Yu et al., who showed that formamide can be used as a growth inhibitor to prevent the stacking of the MgAl-LDH sheets [53].

As was described in Sections 2.2 and 2.3 the synthesis of the stacked catalyst configuration was performed by immobilization of MgAl LDH-NSs on ZrO_2 , calcination followed by wet impregnation of Ni, see Scheme 1. The BET (Brunauer–Emmett–Teller) surface area (SA) of the support materials ZrO_2 , calcined NS/Zr, and mixed oxide derived from LDH (MO) was 6, 9 and 144 m²/g, respectively. Notably, the MO support had a 16 and 24-fold higher surface area than NS/Zr and ZrO_2 , respectively. The similar surface area measured for the NS/Zr and ZrO_2 supports suggest that the NSs are mostly lying flat with the basal plane facing the ZrO_2 surface. This is in contrast to a case where the NS will largely arrange perpendicular to the ZrO_2 surface in which we would expect to have significantly higher surface area compared to ZrO_2 .

To evaluate the coverage NSs on the ZrO_2 surface, HR-SEM and HR-TEM analysis of the 2.5Ni/NS/Zr was performed. Figure S3 shows HR-TEM and HR-SEM images of the 2.5Ni/NS/Zr. The images show that most of the surface area of ZrO_2 was covered by the NS. In addition, the images also show that the LDH-NS preserve their sheet-like structure when grafted on the surface of ZrO_2 even after calcinations. The washing treatment for Ni/NS/Zr samples, following Ni impregnation was intended to remove excess Ni precursor, which adsorbed on to the ZrO_2 surface. ICP-OES results for the adsorption of 10 ml 0.25 M Ni precursor on 1 g of either mixed oxide derived from LDH (MO) or ZrO_2 following 1 h gave 44 mg Ni/g_{support} (~30 wt%) and 2.4 mg Ni/g_{support} (~1 wt%), respectively. This strongly indicates that the tendency of the MO to adsorb the Ni precursor is much greater (over 10 fold) than that of ZrO_2 . Notably, in the preparation of the Ni/NS/Zr catalysts pure wet impregnation was used, while to prepare the Ni/Zr the solvent was



Scheme 1. Design and synthesis of catalytic material.

evaporated to precipitate the Ni precursor on the ZrO_2 surface. Hence, the use of a miliQ water wash was sufficient to remove the Ni precursor from the ZrO_2 and not from the MO. The Ni content for all catalysts was determined using ICP-OES, see Table 1. The lower measured Ni content in all the catalysts prepared using NS/Zr, as compared to the expected nominal loading, was the result of the subsequent wash treatment.

This approach allowed a selective impregnation of Ni onto the mixed oxide NSs despite the presence of the underlying ZrO_2 surface. Mixed oxide derived from LDH after calcination (MO) and ZrO_2 were used as control support materials.

The performance of his new hierarchical catalyst configuration was evaluated using undiluted feed (50:50 $\text{CH}_4:\text{CO}_2$) and at a GHSV of $240,000\text{ cm}^3\text{ h}^{-1}\text{ g}_{\text{cat}}^{-1}$. These conditions are comparable to other reported works in published literature [4,17,39,43,55–59].

Because the hierarchical support has a relatively low SA ($9\text{ m}^2/\text{g}$) the loading of Ni on the NS/Zr was expected to have a strong effect on catalytic performance, therefore, a series of catalysts were synthesized: 0.5, 1, 2.5, 5 and 10 wt% Ni on the NS/Zr. The results for MDR at $800\text{ }^\circ\text{C}$, tested at constant catalyst loading, normalized to the wt% of Ni loading are shown in Fig. 1. It is seen that when the reaction was catalyzed by the 5Ni/NS/Zr and 10Ni/NS/Zr the normalized CH_4 and CO_2 conversions for 20 h TOS were consistently lower than the 2.5Ni/NS/Zr by a factor of > 2 and > 4 , respectively, see Fig. 1A–B. The lower normalized activity of the 5 and 10 wt% catalysts as compared to the 2.5 wt% catalyst is attributed to the higher average Ni density of 49, 94 and 21 Ni nm^{-2} , respectively. As seen in the data for the unnormalized reaction data in Figure S4 in Supporting information the conversions of the 2.5, 5 and 10 wt% Ni remained similar despite the significant higher Ni loading in 5 and 10 wt% catalysts. This indicates that in these catalysts the addition of Ni caused clustering of Ni particles on the low surface area support, which effectively kept the Ni surface free for catalysis similar or even slightly lower. This conclusion is supported by the fact that the H_2/CO ratio remained almost the same despite the change in Ni loading, see Fig. 1C.

In contrast, the normalized activity of the 0.5 and 1 wt% Ni, in which the dispersion of Ni is much higher, showed significantly different catalytic behavior. As seen, the normalized conversion of the 0.5Ni/NS/Zr was initially low, gradually increasing over 20 h TOS. The 1Ni/NS/Zr showed a similar initial low activity with a sharp increase in conversion over the first ~ 5 h of reaction. This behavior is attributed to the partial reduction of 0.5 and 1 wt% catalysts during the pretreatment under H_2 at $600\text{ }^\circ\text{C}$ and the further reduction at $800\text{ }^\circ\text{C}$ under the reducing reaction conditions. In addition, it was found that the H_2/CO ratios for the 0.5 and 1 wt% Ni catalyst were significantly different from those of higher loading. The question of the lower normalized activity of the 0.5 and 1 wt% catalysts is being explored and will be reported in due course.

The above results, for the catalysts reduced at $600\text{ }^\circ\text{C}$, demonstrate that the 2.5 wt% Ni is both stable and active, under the reaction conditions used here. Hence, to evaluate the effect of the hierarchical support we focus on the 2.5Ni/NS/Zr catalyst and compare it to results obtained using the 2.5 wt% Ni supported on ZrO_2 (2.5Ni/Zr) and on MO (2.5Ni/MO), see Fig. 2. It can be seen that the 2.5Ni/NS/Zr was over 2 fold more active than 2.5Ni/Zr and about 10 fold more active than 2.5Ni/MO after 20 h TOS. Interestingly, the H_2/CO ratio was 0.2 on 2.5Ni/MO, 0.68 on 2.5Ni/Zr and 0.78 on 2.5Ni/NS/Zr. Results for MDR conducted using the 2.5 wt% Ni catalysts reduced at $800\text{ }^\circ\text{C}$ showed similar trends, see Figure S5 in SI. Altogether, these findings are in agreement with the expected effect of MSI (metal support interaction) on catalytic performance, which should correlate with the extent of interactions between the metal and the support material [60]. To verify that the effect on the catalytic performance was due to the stacking configuration of the NSs on ZrO_2 rather than due to the catalyst composition we ran the MDR over a mechanical mixture of 2.5Ni/MO and ZrO_2 as a control experiment. These results showed that both the activity and selectivity of MDR were the same as those recorded for 2.5Ni/MO, see Figure S6 in SI. This clearly shows that the stacked configuration of the NSs on the ZrO_2 is a prerequisite for obtaining enhanced catalytic performance rather than simply having the same catalyst chemical composition in the reactor. To evaluate the catalytic contribution of bare supports the reaction was carried out using only the LDH derive mixed oxide (MO), the ZrO_2 (Zr) and the NS/ ZrO_2 (NS/Zr) controls. It was found that all three supports were inactive in MDR.

Results for TGA analysis of the spent catalyst following 20 h of reaction are available in Figure S7. The results show that practically no coke accumulated on the 2.5Ni/Zr catalyst while the 2.5Ni/NS/Zr and 2.5Ni/MO catalysts gained $\sim 0.6\text{ wt\%}$ and $\sim 1.4\text{ wt\%}$, respectively. This correlates well the known ability of oxygen ions to transport through the metal oxide in ZrO_2 , which in turn limit surface carbon formation during MDR [38]. It can be seen that the amount of coke accumulated on the 2.5Ni/NS/Zr was at an intermediate level, which supports the mediating effect of the MgAl-MO-NS. However, the amount of surface carbon formation does not coincide with the trend obtained in the H_2/CO ratio. This indicates that the difference is related to the extent to which the RWGS reaction was promoted rather than to the effect of catalyst deactivation. Notably, the results are consistent with the formation of soft carbon, which oxidizes at temperatures in the range of $300\text{--}520\text{ }^\circ\text{C}$ [61], as opposed to graphitic carbon, which oxidizes at temperature greater than $700\text{ }^\circ\text{C}$ [62].

To understand better the mediating effect of the mixed oxide NS the catalysts were further characterized using PXRD, HR-STEM-EDS, H_2 -TPR and XPS. All catalysts were analyzed using powder X-ray diffraction (PXRD), see Fig. 3 and Figure S8. The diffractograms, in Figure S8 in SI, of the bare ZrO_2 and mixed oxide support materials show peaks

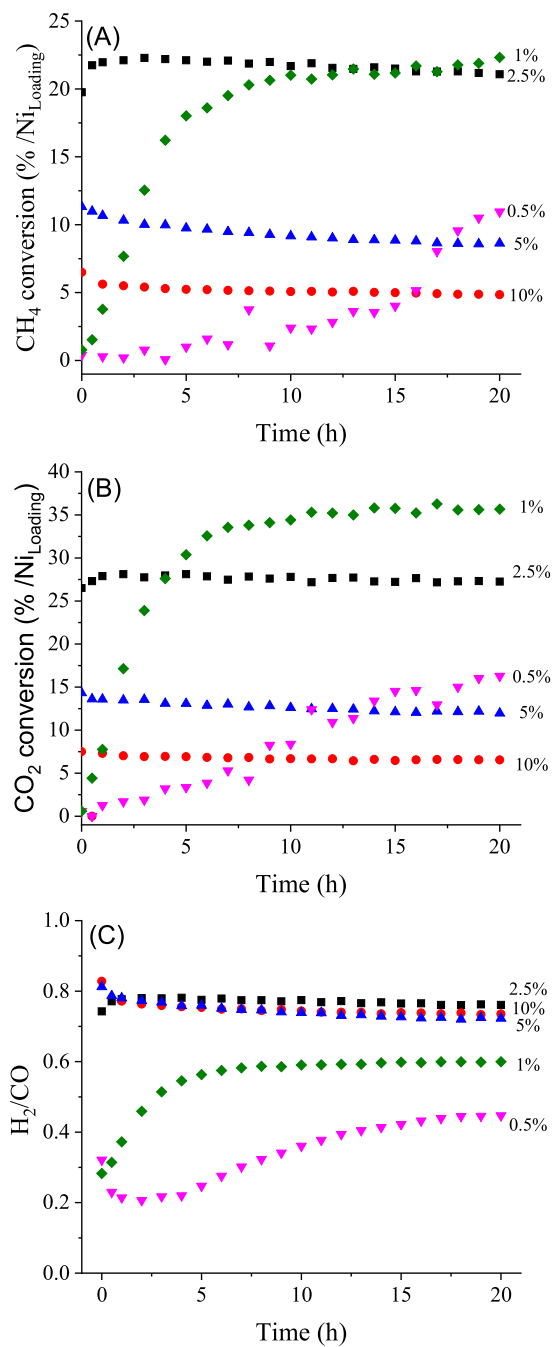


Fig. 1. Effect of Ni loading on the normalized catalytic activity in MDR; ● 10Ni/NS/Zr; ▲ 5Ni/NS/Zr; 2.5Ni/NS/Zr; ◆ 1Ni/NS/Zr; ▼ 0.5Ni/NS/Zr. Catalyst: 25 mg; quartz particles: 175 mg; reduced at: 600 °C, reaction temperature 800 °C; total flow: 100 mL/min (CH₄/CO₂: 50/50).

that are characteristics of pure monoclinic ZrO₂ and MgAl mixed oxide, respectively. The diffractogram of the NS/Zr support was consistent with the composition of mostly monoclinic ZrO₂ with the addition of one small peak at $2\theta = 43.2$, consistent with the (200) reflection plane of the MgAl mixed oxide. The diffractogram of the 2.5Ni/Zr catalyst (a), in Fig. 3B, showed peaks corresponding to the ZrO₂ support and in addition peaks at $2\theta = 37.18$ and 43.24, which correspond to the reflection planes (111) and (200) of NiO (JCPDS file no. #47-4049). In contrast, in the diffractogram of the 2.5Ni/MO catalyst (c) the peaks of the NiO were masked by the peaks of the MO support at $2\theta = 37.02$, 42.97. The diffractogram for the 2.5Ni/NS/Zr was consistent with that of monoclinic ZrO₂ but, no signals were seen for either the MgAl mixed

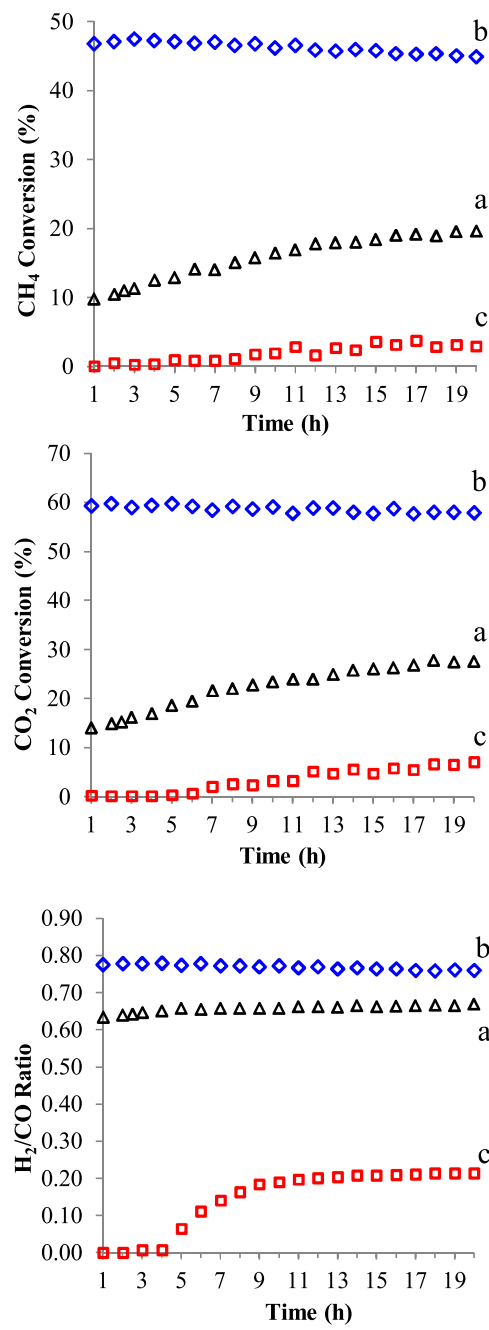


Fig. 2. Catalytic activities of various catalysts with 2.5 wt% Ni loading in MDR; a) 2.5Ni/Zr, b) 2.5Ni/NS/Zr, c) 2.5Ni/MO. Catalyst: 25 mg; quartz particle: 175 mg; reduction condition: 600 °C, 1h, reaction temperature 800 °C; total flow 100 mL/min (CH₄/CO₂: 50/50).

oxide or NiO.

The size of the primary NiO particle, calculated using the Scherrer equation, was 24 nm for the 2.5Ni/Zr. In contrast, in the Ni/MO and Ni/NS/Zr catalysts the masking of the NiO peaks by the MO support prevented calculation of NiO crystal size. On the other hand, comparing the patterns of 2.5Ni/NS/Zr and 2.5Ni/Zr, the absence of NiO peaks at $2\theta = 37.18$ and 43.24 in the former as compared to the latter suggests that the NiO nanocrystallite size in the former was much smaller. The formation of smaller NiO nanoparticles on the NS/Zr as compared to ZrO₂ is attributed to the location of the NiO nanoparticles on the NS of mixed oxide. This conclusion is consistent with previous findings that showed stabilization of smaller Ni nanoparticles by the formation of Ni-O bond in NiO on MgO system [63,64], and for NiO supported on a

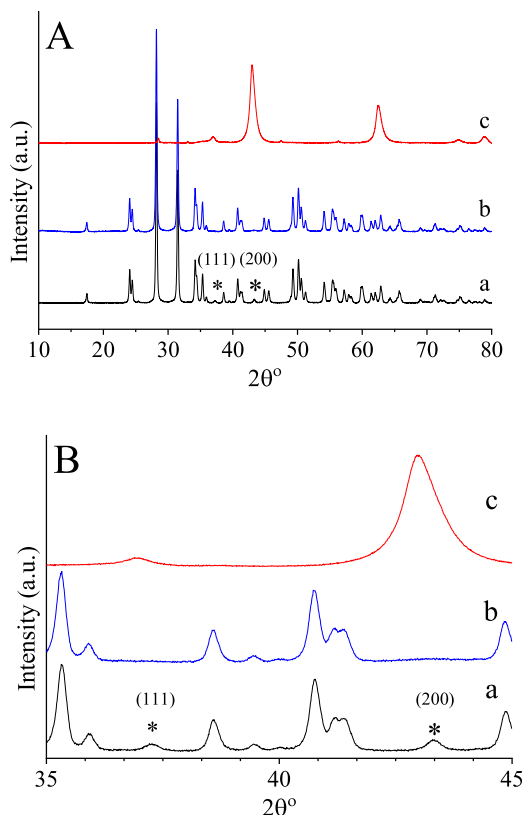


Fig. 3. XRD patterns of the various catalysts, a)2.5Ni/Zr, b)2.5Ni/NS/Zr, c) 2.5Ni/MO A) Diffractograms for $2\theta^\circ = 10\text{--}80$; B) Diffractograms for $2\theta^\circ = 35\text{--}45$ *peaks for NiO.

MgAl mixed oxide [65].

To measure the average size of the Ni nanoparticles we used STEM imaging and elemental mapping of the Ni in the 2.5Ni/Zr, 2.5Ni/MO and 2.5Ni/NS/Zr samples, see Fig. 4. As seen the STEM images of the 2.5Ni/Zr catalyst showed an average Ni particle size of 24–50 nm, see Fig. 4A. These sizes are within range of what was calculated from the PXRD data above. The STEM images of 2.5Ni/NS/Zr catalyst with elemental mapping for Ni, Mg, Al and Zr showed that most of the ZrO_2 surface is covered by MgAl mixed oxide and that the Ni is present in areas with where Mg and Al (yellow arrows) can be found, see Figure S9 in SI. This is in contrast to areas where only Zr can be seen (white arrow) which do not show a Ni signal. Moreover, it can be seen that the signal at the edges of the particle is stronger, which is consistent with the grazing path of the electron beam and the collection of the EDS signal along the exterior of the particle. Unfortunately, because HAADF-STEM-EDS simultaneously collects data from the particle volume it alone cannot be used to show that in the Ni/NS/Zr catalyst the Ni is only on the NS and is absent from the Zr surface. As seen from the HR-STEM images of 2.5Ni/NS/Zr in column (B) the Ni particles are on the order of 2 nm. Measuring a distance of 1.884 nm for 9 crystal planes in that nanoparticle enabled calculating a d-spacing of 0.205 nm, which corresponds to the (200) plane of NiO. Similarly, the images in column (C) of Fig. 4 for NiO in the 2.5Ni/MO catalyst show particle sizes of ~2 nm. The similar sizes of NiO NPs obtained in both 2.5Ni/MO and in 2.5Ni/NS/Zr is surprising given that the former has a 16-fold higher surface area. The smaller nanoparticle size found for the catalysts, in which NiO is supported on either bulk MO or NS/Zr, is attributed to the stabilizing effect of the MgAl mixed oxide support and is consistent with the conclusions drawn from the PXRD analysis. Moreover, the combined observations from STEM-EDS and PXRD supports our conclusion that in the Ni/NS/Zr the Ni phase was well dispersed on the NS compare to ZrO_2 .

The effect of the support on the reducible properties of the NiO phase was tested by analyzing the catalysts using H₂-TPR (temperature programmed reduction); results are summarized in Fig. 5 and Table 2. The TPR profiles for the bare support materials ZrO_2 , MO and NS/Zr showed only mild reduction peaks at around 500 °C–600 °C (refer to Figure S10). In general, during TPR measurements under a linear heating profile the reduction temperature of supported metal catalysts is affected by both the size of the metal oxide particle and the magnitude of the MSI. For the same support, when the size of the Ni nanoparticle is smaller the reduction peak will appear at a lower temperature than that of larger nanoparticles. However, if a small metal oxide nanoparticle is supported on a strongly interacting support (s-MSI), the reduction peak will appear at a higher temperature than that for the same nanoparticle size on a weakly interacting support (w-MSI). As discussed above and shown by STEM-EDS and PXRD, NiO on MO presents s-MSI while NiO on ZrO_2 gives rise to w-MSI. Hence, it can be expected that the NiO in the 2.5Ni/MO would reduce at a high temperature (e.g. 810 °C), while the NiO in the 2.5Ni/Zr would reduce at a much lower temperature (e.g. 400 °C), see Fig. 5. Importantly, both the 2.5Ni/MO and the 2.5Ni/NS/Zr catalysts did not show any reduction peak around 400 °C, which serves as a strong evidence to the physical location of the Ni particles on the MgAl-MO rather than on the Zr surface in the NS/Zr. Surprisingly, despite the fact that in both 2.5Ni/NS/Zr and 2.5Ni/MO the NiO had a similar ~2 nm particle size and were in contact with the MO, the peak reduction temperature of NiO in the former was ~730 °C, which is 80 °C lower than that of the latter, see Fig. 5.

More detailed analysis of the TPR profiles showed that for all catalysts the amount of H₂ consumed during NiO reduction was well correlated with the Ni loading measured by ICP-OES, see Table 1. The 2.5Ni/Zr catalyst gave a broad peak in the range of 300 to 500 °C, of which the shoulder at ca. 320 °C corresponds to bulk NiO [66] and the intense peak at slightly higher temperature is related to NiO that interacts with ZrO_2 , see Fig. 5. In contrast, the TPR profile of 2.5Ni/NS/Zr showed a broad peak in the starting at 400 °C, Fig. 5 which corresponds to the reduction profile of the support, see Figure S10 in SI. Cross-referencing the conclusions of PXRD and STEM-EDS analysis, which showed that the size of the Ni particles in the 2.5Ni/Zr was distinctly larger (24–50 nm) as compared to that in the 2.5Ni/MO and 2.5Ni/NS/Zr (~2 nm), with the TPR results above clearly shows that the differences in the reduction temperature arose due to changes in MSI. The catalysts degree of reduction in H₂ was calculated by repeating the treatment done prior to running the MDR reaction, see values in Table 2. As seen both the 2.5Ni/Zr and the 2.5Ni/NS/Zr were fully reduced following treatment of 1 h at 600 °C under H₂ while the 2.5Ni/MO was only 72% reduced. These results further exemplify the role of the MO nanosheets in mediating the MSI of between Ni and Zr. 2.5Ni/MO was found to fully reduce when a similar treatment was carried out at 800 °C. The 120% obtained on the 2.5Ni/NS/Zr sample is attributed to measurement error arising from the adsorption of H₂ on the oxide support.

To further investigate the influence of the underlying ZrO_2 on MSI of Ni with the mixed oxide NS, the 2.5Ni/Zr, 2.5Ni/MO and 2.5Ni/NS/Zr catalysts were analyzed by XPS, see Ni 2P_{3/2} spectra in Fig. 6. Comparing the spectra of NiO on the three supports showed an upfield shift. As seen the main peak for NiO on the Ni/Zr is at 855.10 eV and for Ni/MO at 855.72 eV. This is consistent with NiO interacting weakly with the support (e.g. ZrO_2) as compared to a stronger interaction (e.g. MO) [67–69]. The higher BE of NiO on MO is similar to previously reported values for NiO/ MgAl_2O_4 [70]. Notably, the NiO on the NS/Zr support gave an intermediate value of 855.48 eV, which provides further evidence for the mediating effect of the mixed oxide NS in the hierarchical support.

3.2. Apparent activation energy estimation

The results of TPR, XPS and catalytic performance evaluation all

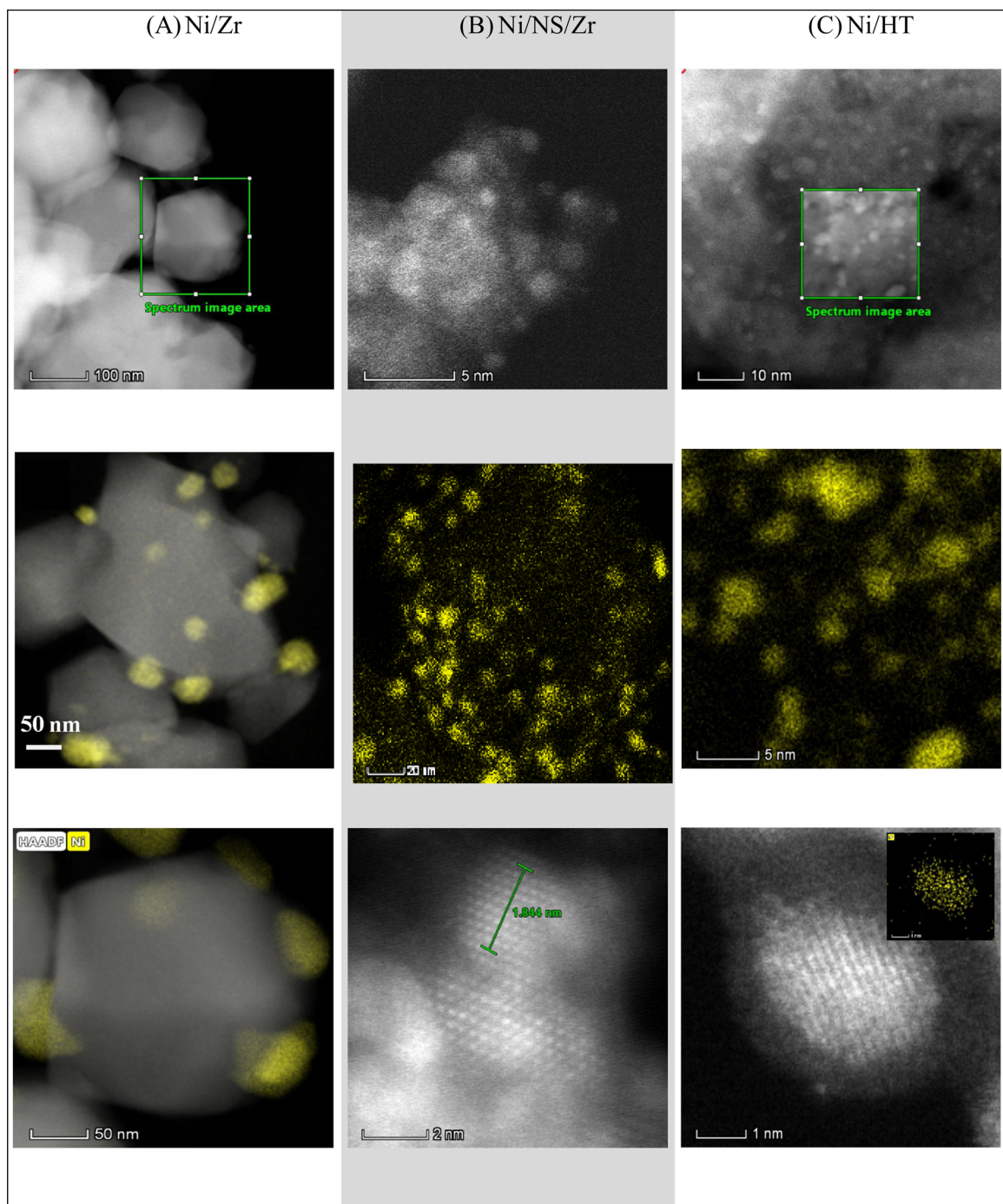


Fig. 4. STEM images of the catalysts with elemental mapping of the Ni: A) 2.5Ni/Zr B) 2.5Ni/NS/Zr C) 2.5Ni/MO. Bright (yellow) in images indicates the background correct EDS signal of Ni.

showed that the MSI of Ni supported on NS/Zr were markedly different from the MSI of Ni supported on MO or ZrO_2 . The changes were attributed to the effect of the thin (~1.9 nm) layer of MgAl mixed oxide, which mediated the interaction between the Ni and the underlying ZrO_2 . If indeed the MSI affected the Ni phase, it should manifest in the apparent activation energy of the reaction. To estimate the apparent activation energy (E_a), the catalysts with 2.5 wt% Ni loading were tested in a temperature range of 680–805 °C, at constant pressure and flow under differential conditions (conversion less than 20%). The apparent activation energies were calculated from the slope of the Arrhenius plot [4,40]. The results are summarized in Table 3 and the full Arrhenius plots are shown in Figure S11 of the SI.

It is generally accepted that the activation of CH_4 takes place on the metal and CO_2 is activated on the support, especially when the support is basic in nature [71,72]. Analyzing the apparent activation energies obtained for CH_4 conversion we found that E_a was: 110 kJ/mol for Ni/MO, 106 kJ/mol for Ni/NS/Zr, and 87 kJ/mol for Ni/Zr. These values are compatible with the previously reported values [4]. The similar E_a values for 2.5Ni/NS/Zr and 2.5Ni/MO indicate that the Ni phase in the 2.5Ni/NS/Zr catalyst is predominantly dispersed on the mixed oxide NS and not on the ZrO_2 (E_a for Ni/Zr is significantly lower). The E_a values calculated based on the CO_2 conversion showed a similar trend: 91 kJ/mol (Ni/MO) > 85 kJ/mol (Ni/NS/Zr) > 69 kJ/mol (Ni/Zr). The lower E_a value obtained for the 2.5Ni/NS/Zr, as compared to the 2.5Ni/MO

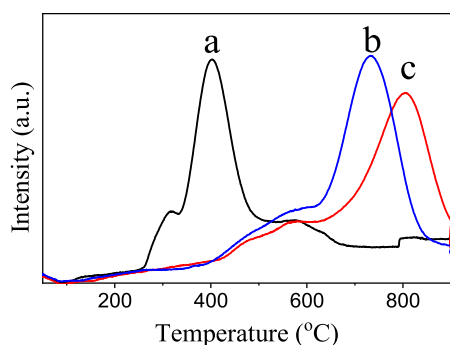


Fig. 5. H₂-TPR inverse profiles for the catalysts a) 2.5Ni/Zr b) 2.5Ni/NS/Zr c) 2.5Ni/MO.

catalyst, may indicate that the CO₂ activation on the mixed oxide NS surface is promoted by the underlying ZrO₂. This latter result coincides well with the result obtained for reaction selectivity. As can be seen in Fig. 2 the H₂/CO ratio of 2.5Ni/NS/Zr is similar to that of 2.5Ni/Zr 0.75 and 0.68, respectively, while the H₂/CO of the 2.5Ni/MO was 0.2. This further shows that despite the lack of direct physical interaction between the Ni and the ZrO₂ in the 2.5Ni/NS/Zr catalyst the H₂/CO ratio trends as that of ZrO₂ rather than the MO on which it is directly supported.

3.3. Catalyst stability

One of the major issues for Ni-catalyzed MDR is the promotion of sintering during the regeneration process. The use of supports that interact strongly with the Ni phase is known to reduce the tendency for sintering but requires a much higher reduction temperature. The unique stacked configuration reported herein allows us to fully reduce the Ni at a significantly lower temperature. The stability of the 2.5Ni/NS/Zr catalyst in MDR at 800 °C was tested and result is shown in Fig. 7. As seen during the first 45 h on stream, there was a mild (~5%) decrease in the conversion of CH₄ and CO₂. The catalyst was then regenerated in-situ by oxidation in air at 600 °C for 1 h followed by reduction in H₂ at 600 °C for 1 h. The temperature was then raised again to 800 °C and the reaction was allowed to proceed for an additional 45 h. As seen, the catalyst regained its original catalytic activity and selectivity. This result indicates that the mechanism for deactivation is related to a reversible effect that occurs with time on stream. Since sintering is not a reversible phenomenon it shows that the most pronounced mechanism for deactivation is catalyst coking. However, when the spent Ni/NS/Zr catalyst was imaged after 250 h on stream using HAADF-STEM-EDS we found evidence for sintering of the Ni particles, see Figure S12. As seen from the images the NiO particle size were found to be 2 nm to 5 nm and even up to 10 nm. Because, the activity was regained after the regeneration the sintering effect was apparently less pronounced. Hence, these results indicate that the Ni supported on the NS/Zr catalyst show good stability.

Table 2

Ni content of various catalysts based on the H₂ consumption.

Sample	Peak reduction temperature [°C]	Total H ₂ consumption [mmol/g]	Ni loading based on H ₂ consumption [wt%] ^a	Ni content Actual (wt%) ^b	Degree of Ni reduction (%) ^a
2.5Ni/MO	810	0.34	2.0	2.29	72 ^c , 103 ^d
2.5Ni/Zr	400	0.35	2.0	2.13	106 ^c
2.5Ni/NS/Zr	733	0.40	2.3	1.89	120 ^c
ZrO ₂	600	0.14	—	—	—
NS/Zr	525, 615	0.17	—	—	—
MO	475, 525	0.15	—	—	—

^a Ni loading was calculated assuming one H₂ molecule per Ni atom after subtracting H₂ consumption of the support.

^b Determined using ICP-OES.

^c Kept for 1 h at the 600 °C under H₂ atmosphere.

^d Kept for 1 h at the 800 °C under H₂ atmosphere.

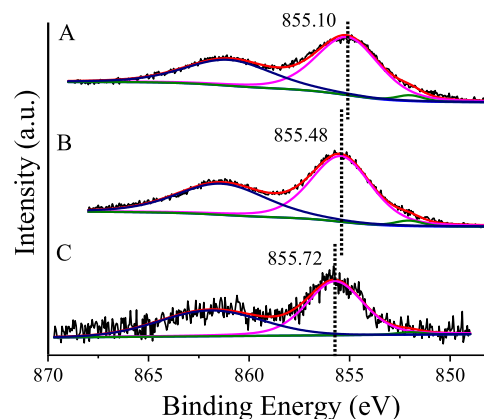


Fig. 6. XPS spectra of Ni (2P_{3/2}) A) 2.5Ni/Zr; B) 2.5Ni/NS/Zr; C) 2.5Ni/MO.

4. Conclusions

This work shows that thin (< 2 nm) nanosheets of MgAl mixed oxide introduced as mediators between Ni nanoparticles and an underlying ZrO₂ support significantly amplified the catalytic performance of Ni in methane dry reforming. We show that this method can be practically used to bridge the gap between a strongly interacting support that promotes stability and a weakly interacting support that enhances activity. It was demonstrated that the 2.5 wt% Ni dispersed on the stacked NS/Zr support is 2 fold more active than Ni/Zr with good stability over 240 h on stream. Comparing our catalytic results to catalyst with similar Ni particles size of ~2 nm [47] shows that even under unoptimized reaction conditions our catalyst gives similar ~46% CH₄ conversion while running at 20-fold higher GHSV.

Furthermore, we show that Ni supported on NS/Zr gave a H₂/CO selectivity similar to that of the underlying ZrO₂, despite the fact that the Ni phase had virtually no physical interaction with the ZrO₂. It was demonstrated that this unique stacked support configuration significantly decreased the reduction temperature of NiO as compared to bulk MO. This allowed for multiple regeneration steps of the catalyst with a total 240 h on stream with only minor signs of Ni degradation by sintering and only mild carbon accumulation. In summary, we have demonstrated a straightforward approach to control metal-support interaction with a dramatic effect on the catalytic performance. It is especially remarkable that the tuning of MSI can be effective even for reactions occurring at 800 °C, which is above the Tamman temperature (T_{Tam}) of the Ni.

Author contributions

The manuscript was written through contributions of all authors. All authors have given approval to the final version of the manuscript.

Table 3Apparent activation energy of CH₄ and CO₂ over various catalysts.

Catalyst	CH ₄ E _a (kJ/mol)	CO ₂ E _a (kJ/mol)
2.5Ni/Zr	87 ± 2.5	69 ± 4.2
2.5Ni/MO	110 ± 2.5	91 ± 1.1
2.5Ni/NS/Zr	106 ± 2.2	85 ± 1.6

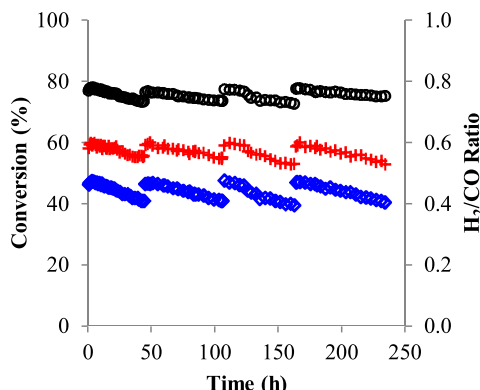


Fig. 7. Stability test of 2.5Ni/NS/Zr for MDR; ◆ CH₄ conversion; + CO₂ conversion; ○ H₂/CO ratio. Catalyst: 25 mg; quart particle: 175 mg; reduction condition: 600 °C, 1 h, reaction temperature 800 °C; total flow 100: mL/min (CH₄/CO₂: 50/50). *regeneration treatment: in-situ oxidation at 600 °C for 1 h followed by in-situ reduction at 600 °C for 1 h.

Acknowledgments

The authors gratefully acknowledge the financial support of the Israeli Ministry of National Infrastructure, Energy and Water Resources grant # 216-11-011, the financial support of the Israeli Science foundation grant #152/11 and the financial support of the Grand Technion Energy Program (GTEP). AT and OG would like to gratefully thank Professor Zhixin Yu and Mr. Dori Kalai from Stavanger University, Norway, for their help in setting up the reaction system. A special thank you is due to Dr. Yaron Kaufman for his help in HR-STEM-EDS imaging.

Appendix A. Supplementary data

Supplementary material related to this article can be found, in the online version, at doi:<https://doi.org/10.1016/j.apcatb.2019.02.040>.

References

- [1] M. Bonomo, A.G. Marrani, V. Novelli, M. Awais, D.P. Dowling, J.G. Vos, D. Dini, Surface properties of nanostructured NiO undergoing electrochemical oxidation in 3-methoxy-propionitrile, *Appl. Surf. Sci.* 403 (2017) 441–447, <https://doi.org/10.1016/j.apsusc.2017.01.202>.
- [2] D. Pakhare, J. Spivey, A review of dry (CO₂) reforming of methane over noble metal catalysts, *Chem. Soc. Rev.* 43 (2014) 7813–7837, <https://doi.org/10.1039/C3CS60395D>.
- [3] D.W. Griffin, M.A. Schultz, E. Irving, P. Road, Fuel and chemical products from biomass syngas: a comparison of gas fermentation to thermochemical conversion routes, *Environ. Prog. Sustain. Energy* 31 (2012) 219–224, <https://doi.org/10.1002/ep>.
- [4] U. Oemar, Y. Kathiraser, L. Mo, X.K. Ho, S. Kawi, CO₂ reforming of methane over highly active La-promoted Ni supported on SBA-15 catalysts: mechanism and kinetic modelling, *Catal. Sci. Technol.* 6 (2016) 1173–1186, <https://doi.org/10.1039/C5CY00906E>.
- [5] B. De Capriatis, P. De Filippis, A. Petrullo, M. Scarsella, Methane dry reforming over nickel perovskite catalysts, *Chem. Eng. Trans.* 43 (2015), <https://doi.org/10.3390/CET1543166>.
- [6] L. Xu, F. Wang, M. Chen, H. Yang, D. Nie, L. Qi, X. Lian, Alkaline-promoted Ni based ordered mesoporous catalysts with enhanced low-temperature catalytic activity toward CO₂ methanation, *RSC Adv.* 7 (2017) 18199–18210, <https://doi.org/10.1039/C7RA01673E>.
- [7] B. Abdullah, N. Azeanni, A. Ghani, D.-V.N. Vo, Recent advances in dry reforming of methane over Ni-based catalysts, *J. Clean. Prod.* 162 (2017) 170–185, <https://doi.org/10.1016/j.jclepro.2017.05.176>.
- [8] L.T. JensRostrup-NielsenDavid, Mechanisms of carbon formation on nickel-containing catalysts, *J. Catal.* 48 (1977) 155–165, [https://doi.org/10.1016/0021-9517\(77\)90087-2](https://doi.org/10.1016/0021-9517(77)90087-2).
- [9] D.S.A. Simakov, M.M. Wright, S. Ahmed, E.M.A. Mokheimerd, Y. Román-Leshkov, Catalysis science & technology review on chemistry, catalysis and system design, *Catal. Sci. Technol.* 5 (2016) 1991–2016, <https://doi.org/10.1039/C4CY01333F>.
- [10] C. Carrara, J. Múnera, E.A. Lombardo, L.M. Cornaglia, Kinetic and stability studies of Ru/La203 used in the dry reforming of methane, *Top. Catal.* 51 (2008) 98–106, <https://doi.org/10.1007/s11244-008-9131-y>.
- [11] P. Ferreira-Aparicio, C. Márquez-Alvarez, I. Rodríguez-Ramos, Y. Schuurman, A. Guerrero-Ruiz, C. Mirodatos, A transient kinetic study of the carbon dioxide reforming of methane over supported Ru catalysts, *J. Catal.* 184 (1999) 202–212, <https://doi.org/10.1006/JCAT.1999.2439>.
- [12] J. Kehres, J.G. Jakobsen, J.W. Andreassen, J.B. Wagner, H. Liu, A. Molenbroek, J. Sehested, I. Chorkendorff, T. Vegge, Dynamical properties of a Ru/MgAl2O4 catalyst during reduction and dry methane reforming, *J. Phys. Chem. C* 116 (2012) 21407–21415, <https://doi.org/10.1021/jp3069656>.
- [13] F.A.J. Al-Doghachi, A. Islam, Z. Zainal, M.I. Saiman, Z. Embong, Y.H. Taufiq-Yap, High coke-resistance Pt/Mg1-xNiO catalyst for dry reforming of methane, *PLoS One* 11 (2016) e0145862, <https://doi.org/10.1371/journal.pone.0145862>.
- [14] M. Safariamin, L.H. Tidahy, E. Abi-Aad, S. Siffert, A. Abouka, Dry reforming of methane in the presence of ruthenium-based catalysts, *Comptes Rendus - Chim.* 12 (2009) 748–753, <https://doi.org/10.1016/j.crci.2008.10.021>.
- [15] Z. Zhang, X.E. Verykios, S.M. MacDonald, S. Affrossman, Comparative study of carbon dioxide reforming of methane to synthesis gas over Ni/La2O3 and conventional nickel-based catalysts, *J. Phys. Chem. C* 100 (1996) 744–754, <https://doi.org/10.1021/jp951809e>.
- [16] H.S. Whang, M.S. Choi, J. Lim, C. Kim, I. Heo, T.-S. Chang, H. Lee, Enhanced activity and durability of Ru catalyst dispersed on zirconia for dry reforming of methane, *Catal. Today* 293–294 (2017) 122–128, <https://doi.org/10.1016/j.cattod.2016.12.034>.
- [17] W.Y. Kim, Y.H. Lee, H. Park, Y.H. Choi, M.H. Lee, J.S. Lee, Coke tolerance of Ni/Al2O3 nanosheet catalyst for dry reforming of methane, *Catal. Sci. Technol.* 6 (2016) 2060–2064, <https://doi.org/10.1039/C6CY00017G>.
- [18] J.L. Ewbank, L. Kovarik, F.Z. Diallo, C. Sievers, Effect of metal-support interactions in Ni/Al2O3 catalysts with low metal loading for methane dry reforming, *Appl. Catal. A Gen.* 494 (2015) 57–67, <https://doi.org/10.1016/j.apcata.2015.01.029>.
- [19] K. Mette, S. Kühl, A. Tarasov, M.G. Willinger, J. Kröhnert, S. Wrabetz, A. Trunschke, M. Scherzer, F. Girsigdes, H. Düdder, K. Kähler, K.F. Ortega, M. Muhrer, R. Schlögl, M. Behrens, T. Lunkenbein, High-temperature stable Ni nanoparticles for the dry reforming of methane, *ACS Catal.* 6 (2016) 7238–7248, <https://doi.org/10.1021/acscatal.6b01683>.
- [20] A. Kambolis, H. Matralis, A. Trovarelli, C. Papadopoulou, Ni/CeO₂-ZrO₂ catalysts for the dry reforming of methane, *Appl. Catal. A Gen.* 377 (2010) 16–26, <https://doi.org/10.1016/j.apcata.2010.01.013>.
- [21] S.J. Blanksby, G.B. Ellison, Bond dissociation energies of organic molecules, *Acc. Chem. Res.* 36 (2003) 255–263, <https://doi.org/10.1021/ar020230d>.
- [22] X. Du, D. Zhang, R. Gao, L. Huang, L. Shi, J. Zhang, Design of modular catalysts derived from NiMgAl-LDH@m-SiO₂ with dual confinement effects for dry reforming of methane, *Chem. Commun.* 49 (2013) 6770–6772, <https://doi.org/10.1039/C3CC42418A>.
- [23] B.M. Choudary, N.S. Chowdari, S. Madhi, M.L. Kantam, A trifunctional catalyst for the synthesis of chiral diols, *Angew. Chem. Int. Ed.* 40 (2001) 4619–4623, [https://doi.org/10.1002/1521-3773\(20011217\)40:24<4619::AID-ANIE4619>3.0.CO;2-U](https://doi.org/10.1002/1521-3773(20011217)40:24<4619::AID-ANIE4619>3.0.CO;2-U).
- [24] S. Takenaka, H. Umebayashi, E. Tanabe, H. Matsune, M. Kishida, Specific performance of silica-coated Ni catalysts for the partial oxidation of methane to synthesis gas, *J. Catal.* 245 (2007) 392–400, <https://doi.org/10.1016/j.jcat.2006.11.005>.
- [25] M. Cargnello, V.V.T. Doan-Nguyen, T.R. Gordon, R.E. Diaz, E.A. Stach, R.J. Gorte, P. Fornasiero, C.B. Murray, Control of metal nanocrystal size reveals metal-support interface role for ceria catalysts, *Science (Washington DC U. S.)* 341 (2013) 771–773, <https://doi.org/10.1126/science.1240148>.
- [26] A.M. Argo, J.F. Odzak, F.S. Lai, B.C. Gates, Observation of ligand effects during alkene hydrogenation catalysed by supported metal clusters, *Nature* 415 (2002) 623–626 <http://search.proquest.com/docview/204514440?accountid=27233>.
- [27] J.A. Farmer, C.T. Campbell, Ceria maintains smaller metal catalyst particles by strong metal-support bonding, *Science (Washington DC U. S.)* 329 (2010) 933–936, <https://doi.org/10.1126/science.1191778>.
- [28] M. Cargnello, P. Fornasiero, R.J. Gorte, Opportunities for tailoring catalytic properties through metal-support interactions, *Catal. Lett.* 142 (2012) 1043–1048, <https://doi.org/10.1007/s10562-012-0883-4>.
- [29] A.L.M. da Silva, J.P. den Breejen, L.V. Mattos, J.H. Bitter, K.P. de Jong, F.B. Noronha, Cobalt particle size effects on catalytic performance for ethanol steam reforming – smaller is better, *J. Catal.* 318 (2014) 67–74, <https://doi.org/10.1016/j.jcat.2014.07.020>.
- [30] G.L. Haller, D.E. Resasco, H.P.D.D. Eley, B.W. Paul (Eds.), *Metal-Support Interaction: Group VIII Metals and Reducible Oxides*, *Adv. Catal.*, Academic Press, 1989, pp. 173–235, [https://doi.org/10.1016/S0360-0564\(08\)60018-8](https://doi.org/10.1016/S0360-0564(08)60018-8).
- [31] S.J. Tauster, S.C. Fung, R.L. Garten, Strong metal-support interactions. Group 8 noble metals supported on titanium dioxide, *J. Am. Chem. Soc.* 100 (1978) 170–175, <https://doi.org/10.1021/ja0046902>.
- [32] A.M. Abdel-Mageed, D. Widmann, S.E. Olesen, I. Chorkendorff, J. Biskupek, R.J. Behm, Selective CO methanation on Ru/TiO₂ catalysts: role and influence of metal-support interactions, *ACS Catal.* 5 (2015) 6753–6763, <https://doi.org/10.1021/acscatal.5b01520>.

- [33] Y. Wang, Y. Zhai, D. Pierre, M. Flytzani-Stephanopoulos, Silica-encapsulated platinum catalysts for the low-temperature water-gas shift reaction, *Appl. Catal. B Environ.* 127 (2012) 342–350, <https://doi.org/10.1016/j.apcatb.2012.08.038>.
- [34] Z. Zuo, S. Liu, Z. Wang, C. Liu, W. Huang, J. Huang, P. Liu, Dry reforming of methane on single-site Ni/MgO catalysts: importance of site confinement, *ACS Catal.* 8 (2018) 9821–9835, <https://doi.org/10.1021/acscatal.8b02277>.
- [35] Y. Cao, P. Maitarad, M. Gao, T. Taketsugu, H. Li, T. Yan, L. Shi, D. Zhang, Defect-induced efficient dry reforming of methane over two-dimensional Ni/h-boron nitride nanosheet catalysts, *Appl. Catal. B Environ.* 238 (2018) 51–60, <https://doi.org/10.1016/j.apcatb.2018.07.001>.
- [36] M. Lu, J. Fang, L. Han, K. Faungnawakij, H. Li, S. Cai, L. Shi, H. Jiang, D. Zhang, Coke-resistant defect-confined Ni-based nanosheet-like catalysts derived from halloysites for CO₂ reforming of methane, *Nanoscale* 10 (2018) 10528–10537, <https://doi.org/10.1039/c8nr02006j>.
- [37] Y. Cao, M. Lu, J. Fang, L. Shi, D. Zhang, Hexagonal boron nitride supported mesoSiO₂-confined Ni catalysts for dry reforming of methane, *Chem. Commun.* 53 (2017) 7549–7552, <https://doi.org/10.1039/c7cc02007d>.
- [38] J.W. Han, J.S. Park, M.S. Choi, H. Lee, Uncoupling the size and support effects of Ni catalysts for dry reforming of methane, *Appl. Catal. B Environ.* 203 (2017) 625–632, <https://doi.org/10.1016/j.apcatb.2016.10.069>.
- [39] R. Debek, M. Motak, D. Duraczyska, F. Launay, M.E. Galvez, T. Grzybek, P. Da Costa, Methane dry reforming over hydrotalcite-derived Ni-Mg-Al mixed oxides: the influence of Ni content on catalytic activity, selectivity and stability, *Catal. Sci. Technol.* 6 (2016) 6705–6715, <https://doi.org/10.1039/C6CY00906A>.
- [40] S. Wang, G.Q.(Max) Lu*, G.J. Millar, Carbon dioxide reforming of methane to produce synthesis gas over metal-supported catalysts: State of the art, *Energy Fuels.* 10 (1996) 896–904, <https://doi.org/10.1021/EF950227T>.
- [41] F. Touahra, M. Sehailia, W. Ketir, K. Bachari, R. Cheboub, M. Trari, O. Cherifi, D. Halliche, Effect of the Ni/Al ratio of hydrotalcite-type catalysts on their performance in the methane dry reforming process, *Appl. Petrochem. Res.* 6 (2016) 1–13, <https://doi.org/10.1007/s13203-015-0109-y>.
- [42] A.R. González, Y.J.O. Ascencios, E.M. Assaf, J.M. Assaf, Dry reforming of methane on Ni-Mg-Al nano-spheroid oxide catalysts prepared by the sol-gel method from hydrotalcite-like precursors, *Appl. Surf. Sci.* 280 (2013) 876–887, <https://doi.org/10.1016/j.apsusc.2013.05.082>.
- [43] S.A. Theofanidis, V.V. Galvita, H. Poelman, G.B. Marin, Enhanced carbon-resistant dry reforming Fe-Ni catalyst: role of Fe, *ACS Catal.* 5 (2015) 3028–3039, <https://doi.org/10.1021/acscat.5b00357>.
- [44] L. Li, D.H. Anjum, H. Zhu, Y. Saif, P.V. Laveille, L. D’Souza, J.-M. Basset, Synergistic effects leading to coke-resistant NiCo bimetallic catalysts for dry reforming of methane, *ChemCatChem.* 7 (2015) 427–433, <https://doi.org/10.1002/cctc.201402921>.
- [45] S. Li, C. Zhang, Z. Huang, G. Wu, J. Gong, A Ni@ZrO₂ nanocomposite for ethanol steam reforming: enhanced stability via strong metal–oxide interaction, *Chem. Commun.* 43 (2013) 4226–4228, <https://doi.org/10.1039/c2cc37109j>.
- [46] S. Das, J. Ashok, Z. Bian, N. Dewangan, M.H. Wai, Y. Du, A. Borgna, K. Hidajat, S. Kawi, Ceria sandwiched Ni core – shell catalyst for low temperature dry reforming of biogas : coke resistance and mechanistic insights, *Appl. Catal. B : Environ. Silica* 230 (2018) 220–236, <https://doi.org/10.1016/j.apcatb.2018.02.041>.
- [47] J. Woo, J. Seong, M. Suk, H. Lee, Environmental uncoupling the size and support effects of Ni catalysts for dry reforming of methane, *Appl. Catal. B Environ.* 203 (2017) 625–632, <https://doi.org/10.1016/j.apcatb.2016.10.069>.
- [48] S. Li, J. Gong, Chem soc rev strategies for improving the performance and stability of Ni-based catalysts for reforming reactions, *Chem. Soc. Rev. Chem. Soc. Rev.* 43 (2014) 7239–7456.
- [49] S.S. Chan, I.E. Wachs, L.L. Murrell, L. Wang, W.K. Hall, In situ laser Raman spectroscopy of supported metal oxides, *J. Phys. Chem.* 88 (1984) 5831–5835, <https://doi.org/10.1021/j150668a018>.
- [50] E.I. Ko, F.H. Rogan, Metal-support interactions for nickel supported on a tetania-silica surface phase oxide, *Chem. Eng. Commun.* 55 (1987) 139–148, <https://doi.org/10.1080/00986448708911923>.
- [51] E.I. Ko, R. Bafrali, N.T. Nuhfer, N.J. Wagner, The use of a niobia-silica surface phase oxide in studying and varying metal-support interactions in supported nickel catalysts, *J. Catal.* 95 (1985) 260–270.
- [52] A.P. Tathod, O.M. Gazit, Fundamental insights into the nucleation and growth of Mg-Al layered double hydroxides nanoparticles at Low temperature, *Cryst. Growth Des.* 16 (2016) 6709, <https://doi.org/10.1021/acs.cgd.6b01272>.
- [53] J. Yu, B.R. Martin, A. Clearfield, Z. Luo, L. Sun, One-step direct synthesis of layered double hydroxide single-layer nanosheets, *Nanoscale* 7 (2015) 9448–9451, <https://doi.org/10.1039/C5NR01077B>.
- [54] F.L.A. S.D. I, W. George (Ed.), *Structure Analysis by Small-Angle X-Ray and Neutron Scattering*, Plenum Press, New York, 1987.
- [55] A. Wolfbeisser, O. Sophiphun, J. Bernardi, J. Wittayakun, K. Föttinger, G. Rupprechter, Methane dry reforming over ceria-zirconia supported Ni catalysts, *Catal. Today* 277 (2016) 234–245, <https://doi.org/10.1016/j.cattod.2016.04.025>.
- [56] H. Liu, D. Wierzbicki, R. Debek, M. Motak, T. Grzybek, P. Da Costa, M.E. Galvez, La-promoted Ni-hydrotalcite-derived catalysts for dry reforming of methane at low temperatures, *Fuel* 182 (2016) 8–16, <https://doi.org/10.1016/j.fuel.2016.05.073>.
- [57] L. Xinsheng, J. Chang, M. Tian, S. Park, CO₂ reforming of methane over modified Ni/ZrO₂ catalysts, *Appl. Organomet. Chem.* 15 (2001) 109–112.
- [58] V.M. Gonzalez-Delacruz, R. Pereñiguez, F. Ternero, J.P. Holgado, A. Caballero, Modifying the size of nickel metallic particles by H₂/CO treatment in Ni/ZrO₂ methane dry reforming catalysts, *ACS Catal.* 1 (2011) 82–88, <https://doi.org/10.1021/cs100116m>.
- [59] N. Pegios, V. Bliznuk, S.P. Unte, J.M. Schneider, R. Palkovits, K. Simeonov, Comparative study on La-promoted Ni/g-Al₂O₃ for methane dry reforming – spray drying for enhanced nickel dispersion and strong metal– support interactions, *RSC Adv.* 8 (2018) 606, <https://doi.org/10.1039/c7ra06570a>.
- [60] R. Dębek, M. Motak, T. Grzybek, M. Galvez, P. Da Costa, A short review on the catalytic activity of hydrotalcite-derived materials for dry reforming of methane, *Catalysts* 7 (2017) 32, <https://doi.org/10.3390/catal7010032>.
- [61] E. le Saché, L. Pastor-Pérez, D. Watson, A. Sepúlveda-Escribano, T.R. Reina, Ni stabilised on inorganic complex structures: superior catalysts for chemical CO₂recycling via dry reforming of methane, *Appl. Catal. B Environ.* 236 (2018) 458–465, <https://doi.org/10.1016/j.apcatb.2018.05.051>.
- [62] H. Düdder, K. Kähler, B. Krause, K. Mette, S. Kühl, M. Behrens, V. Scherer, M. Mühlner, The role of carbonaceous deposits in the activity and stability of Ni-based catalysts applied in the dry reforming of methane, *Catal. Sci. Technol.* 4 (2014) 3317–3328, <https://doi.org/10.1039/c4cy00409d>.
- [63] M.C.J. Bradford, M.A. Vannice, Catalytic reforming of methane with carbon dioxide over nickel catalysts II. Reaction kinetics, *Appl. Catal. A Gen.* 142 (1996) 97–122, [https://doi.org/10.1016/0926-860X\(96\)00066-X](https://doi.org/10.1016/0926-860X(96)00066-X).
- [64] Y.H. Hu, E. Ruckenstein, An optimum NiO content in the CO₂ reforming of CH₄ with NiO/MgO solid solution catalysts, *Catal. Lett.* 36 (1996) 145–149, <https://doi.org/10.1007/BF000807611>.
- [65] T. Shishido, M. Sukanobu, H. Morioka, R. Furukawa, H. Shirahase, K. Takehira, CO₂ reforming of CH₄ over Ni/Mg-Al oxide catalysts prepared by solid phase crystallization method from Mg-Al hydrotalcite-like precursors, *Catal. Lett.* 73 (2001) 21–26, <https://doi.org/10.1023/A:1009066017469>.
- [66] C. Ding, G. Ai, K. Zhang, Q. Yuan, Y. Han, X. Ma, J. Wang, S. Liu, Coking resistant Ni/ZrO₂@SiO₂ catalyst for the partial oxidation of methane to synthesis gas, *Int. J. Hydrogen Energy.* 40 (2015) 6835–6843, <https://doi.org/10.1016/j.ijhydene.2015.03.094>.
- [67] J. Yang, J. Ren, H. Guo, X. Qin, B. Han, J. Lin, Z. Li, The growth of Ni n clusters and their interaction with cubic, monoclinic, and tetragonal ZrO₂ surfaces—a theoretical and experimental study, *RSC Adv.* 5 (2015) 59935–59945, <https://doi.org/10.1039/C5RA07738A>.
- [68] B. Pawelec, S. Damyanova, K. Arishtiroya, J.L.G. Fierro, L. Petrov, Structural and surface features of PtNi catalysts for reforming of methane with CO₂, *Appl. Catal. A Gen.* 323 (2007) 188–201, <https://doi.org/10.1016/j.apcata.2007.02.017>.
- [69] H. Shang, K. Pan, L. Zhang, B. Zhang, X. Xiang, Enhanced activity of supported Ni catalysts promoted by Pt for Rapid reduction of aromatic nitro compounds, *Nanomaterials.* 6 (2007) 103, <https://doi.org/10.3390/nano6060103>.
- [70] H.-W. Kim, K.-M. Kang, H.-Y. Kwak, J.H. Kim, Preparation of supported Ni catalysts on various metal oxides with core/shell structures and their tests for the steam reforming of methane, *Chem. Eng. J.* 168 (2011) 775–783, <https://doi.org/10.1016/j.cej.2010.11.045>.
- [71] J.H. Bitter, K. Seshan, J.A. Lercher, Mono and bifunctional pathways of CO₂/CH₄ reforming over Pt and Ru based catalysts, *J. Catal.* 176 (1998) 93–101, <https://doi.org/10.1006/JCAT.1998.2022>.
- [72] P. Ferreira-Aparicio, I. Rodríguez-Ramos, J. Anderson, A. Guerrero-Ruiz, Mechanistic aspects of the dry reforming of methane over ruthenium catalysts, *Appl. Catal. A Gen.* 202 (2000) 183–196, [https://doi.org/10.1016/S0926-860X\(00\)00525-1](https://doi.org/10.1016/S0926-860X(00)00525-1).